Spatiotemporal Variations of Growing-Season NDVI Associated with Climate Change in Northeastern China's Permafrost Zone

Jinting Guo[1, 2], Yuanman Hu[1], Zaiping Xiong[1], Xiaolu Yan[1, 2], Baihui Ren[1, 2], Rencang Bu[1]*

[1]CAS Key Laboratory of Forest Ecology and Management, Institute of Applied Ecology, Chinese Academy of Sciences, No. 72, Wenhua Road, 110016, Shenyang, China
[2]University of Chinese Academy of Sciences, No. 19, Yuquan Road, 100049, Beijing, China

Abstract

Vegetation is an essential component of terrestrial ecosystems, and it plays an important role in regulating climate change, the carbon cycle, and energy exchange. And permafrost is extremely sensitive to climate change. In particular, aboveground vegetation on permafrost has great sensitivity to that change. The permafrost zone of northeastern China, within middle and high latitudes of the northern hemisphere, is the second-largest region of permafrost in China. It is at the southern edge of the Eurasian cryolithozone. This study analyzes growing-season spatiotemporal variation of the normalization difference vegetation index (NDVI) in this permafrost zone and the correlation between NDVI and climate variables during 1981-2014. Mean growing-season NDVI significantly increased by 0.0028 yr^{-1} over the entire permafrost zone. The spatial dynamics of vegetation cover in the zone had strong heterogeneity on the pixel scale. Pixels that showed increasing trends accounted for 80% of the permafrost area, and were mostly found in the permafrost zone with the exception of western steppe regions. Pixels that showed decreasing trends (approximately 20% of the permafrost area) were mainly in the cultivated and steppe portions of the study area. Our results indicated that temperature was the dominant influence on vegetation growth during the growing season in most permafrost zones.

Introduction

Vegetation is an essential component of terrestrial ecosystems, and is important in regulating climate change, the carbon cycle, and energy exchange via biophysical factors such as photosynthesis, evapotranspiration, surface albedo, and roughness [1-4]. Vegetation has obvious interannual and seasonal variations that are recognized as indicators for the detection of climate trends in global change studies [5-8]. Thus, we can better understand and simulate the dynamic characteristics of terrestrial ecosystems and reveal the regulation of global change by monitoring long-term vegetation variations. Studies of the

*e-mail: brc_landscape@163.com, burc@iae.ac.cn

spatiotemporal variations of vegetation activities caused by climate change, including plant phenology [9-13], net primary productivity [14-17], vegetation cover [18-22], biomass [23-24], and carbon process models [25], have used various methods. These studies have revealed that vegetation activities have increased at middle and high latitudes of the northern hemisphere over the past few decades.

Remote sensing is a powerful and useful approach to investigating vegetation dynamics. The satellite-derived normalized difference vegetation index (NDVI), which is defined as a ratio of near-infrared and red visible reflectance, is an indicator of vegetation cover, productivity, and growth [26]. A large NDVI value is equivalent high green plant density [20]. NDVI has been broadly used to detect characteristics of vegetation dynamics because of its strong correlation with biophysical and biochemical variables, such as plant coverage, leaf area, chlorophyll density, biomass, and growth. There are various available NDVI datasets, such as AVHRR NDVI, MODIS NDVI, and SPOT VEG NDVI [13, 16-18, 27-28]. Most studies focus on vegetation dynamics by using a single NDVI dataset. Such a single data resource is limited to analysis of a long-term NDVI sequence. Therefore, it is valuable to develop a consistent long-term dataset from the 1980s through recent years, combining advanced very high resolution radiometer (AVHRR) NDVI and moderate resolution imaging radiometer (MODIS) NDVI.

Vegetation variations have been shown to be correlated with climate change. Ichii et al. found significant correlation between interannual change of NDVI and temperature at middle and high latitudes of the northern hemisphere, consistent with Zhou et al. [5, 29]. At these latitudes, the permafrost zone of northeastern China is the second largest expanse of permafrost in the country and is at the southern edge of the Eurasian cryolithozone [30]. The zone is thermally unstable and ecologically sensitive to global climate change [31]. Some studies have suggested that vegetation growth in most areas of China has increased over the past few decades [27, 32-33]. However, these studies mainly dealt with vegetation responses to climate variables on a national scale. There have been few detailed studies at the regional scale, such as the permafrost zone of northeastern China. Therefore, a long-term NDVI dataset is needed to detect vegetation dynamics and correlation between NDVI and climate variables.

The major aim of this study was to probe spatiotemporal variations of NDVI associated with climate in the permafrost zone of northeastern China from 1981 to 2014 based on satellite and climate datasets. We address the following questions:

– How did the vegetation cover (NDVI) vary spatiotemporally in the permafrost zone over a 34-year period?
– Which climate variable (temperature or precipitation) determined the vegetation change?

Our result serves as a guide for managing forest in the permafrost region.

Our study focuses on growing-season NDVI and so avoids outlier NDVI values caused by winter snow cover [33-35]. Here, the growing season is defined as April through October. We determine mean growing-season NDVI to detect variations of vegetation related to climate change.

Materials and Methods

Study Area

The permafrost region studied is in the northernmost part of northeastern China. It extends from 115°52′E to 135°09′E and 46°30′N to 53°30′N, with an area of ~42 million hectares (Fig. 1). The climate regime is characterized by long periods of dry and cold in winter, and short moist and hot periods in summer. Annual average temperatures range from -5ºC to 4ºC (Fig. 2a), and annual precipitation is between 261 and 599 mm (Fig. 2b). The region is mainly covered by forest that is dominated by larch and white birch, and there are small proportions of shrubs, woodland, steppe, meadow, swamp, and cultivated land intermixed (Fig. 1).

NDVI Datasets

We used two datasets, the land long term data record (LTDR) NDVI (AVH13C1) for 1981-99 and MODIS NDVI (MOD13C2) for 2000-14, to depict the spatiotemporal variation of growing-season vegetation cover in the permafrost region of northeastern China during 1981-2014. LTDR AVH13C1 products are supported by the LDTR project, which is funded as part of the National Aeronautics and Space Administration (NASA) Earth
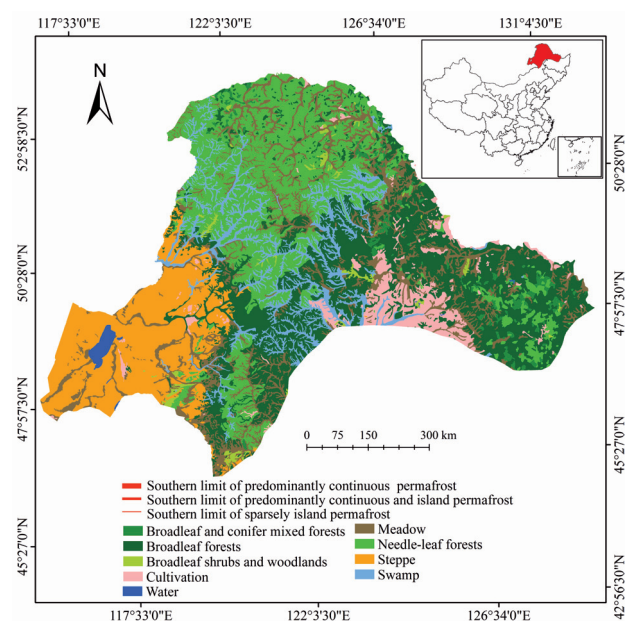

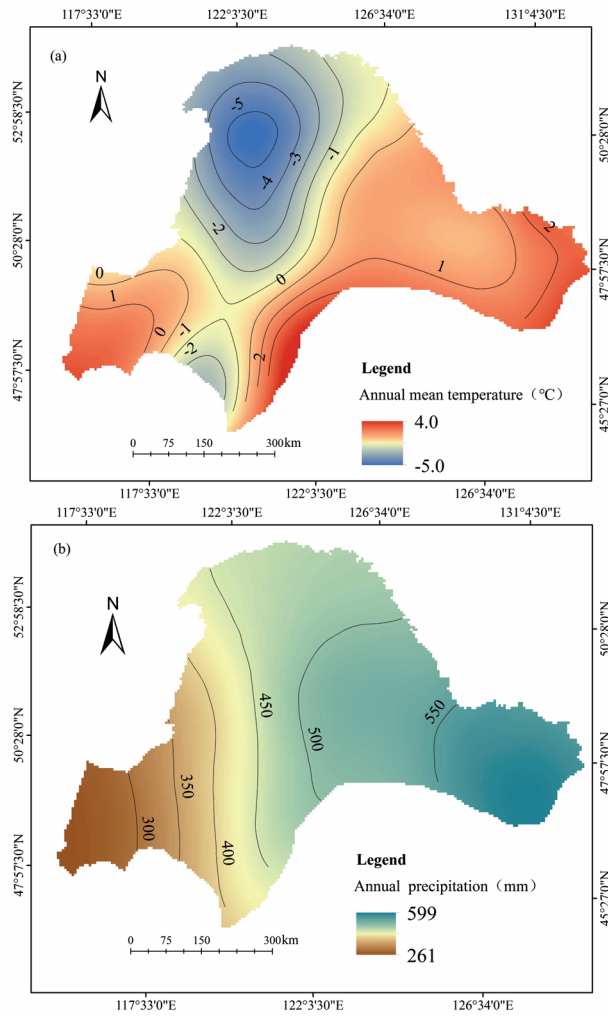Fig. 1. Location and vegetation types of permafrost zone in northeastern China.

Fig. 2. Spatial patterns of a) annual mean temperature and b) precipitation in permafrost zone during 1981-2014.
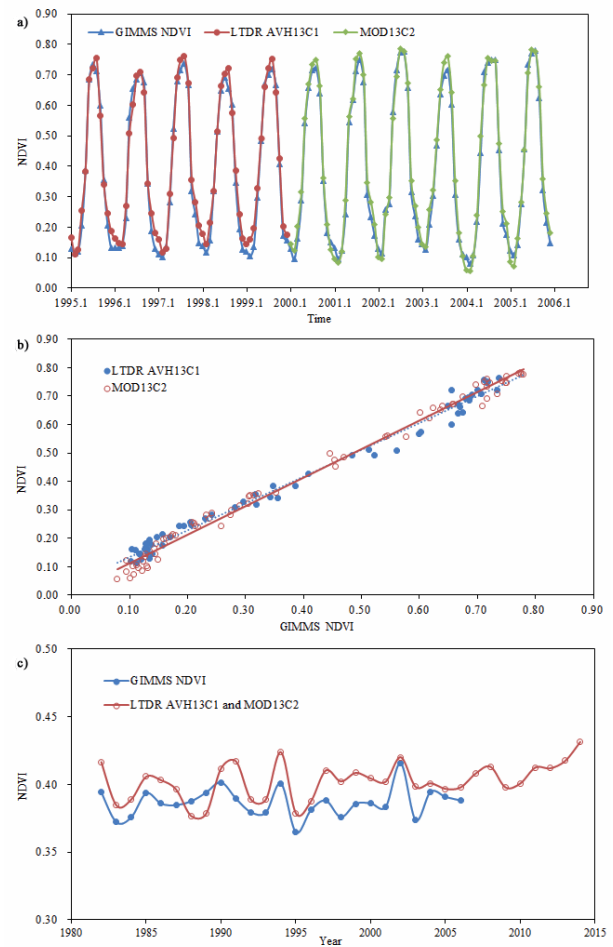

Fig. 3. Comparison of NDVI time sequences obtained from LTDR AVH13C1, MODIS MOD13C2, and GIMMS NDVI for the permafrost region: a) monthly NDVI time series of the three datasets, 1995 to 2005; b) AVH13C1 (blue) and MOD13C2 (red) versus GIMMS NDVI – the red line represents regression that passes through the origin; and c) Annual NDVI time series of the three datasets from 1982 to 2006 (the longest time series of GIMMS NDVI was provided from July 1981 through December 2006).

Science Research, Education, and Application Solution Network. A project objective is to derive consistent and long-term datasets from the AVHRR series satellites (NOAA 7, 9, 11, 14, and 16) [36] and MODIS apparatus for research into global climate change [20, 37]. LTDR AVH13C1 products include daily NDVI data produced for the period 1981-99 with spatial pixel resolution 0.05°, which are preceded by an improved atmospheric correction scheme and bidirectional reflectance distribution function correction [37]. The LTDR dataset and product documents can be downloaded at ltdr.nascom. nasa.gov/cgi-bin/ltdr/ltdrPage.cgi. MODIS has been a key sensor aboard the Terra (generally known as EOS AM-1) and Aqua (generally known as EOS PM-1) satellites from 2000 onward, and provide the opportunity to monitor earth's terrestrial photosynthetic vegetation activity in support of phonologic, change detection, and biophysical interpretation [38-39]. The MOD13C2 datasets are cloud-free spatial composites of the gridded 16-day, 1-km NDVI (MOD13A2) [40], and are provided monthly on a level-3 product geographic climate modeling grid, with a projected spatial pixel resolution of 0.05°. These data

may be obtained from the NASA Level 1 and Atmosphere Archive and Distribution System site (ladsweb.nascom. nasa.gov).

Both datasets involve atmospheric calibration and geometric corrections, especially errors produced by satellite alternation, to ensure data quality [20, 38]. MOD13C2 monthly dataset composites were generated using the maximum value composite (MVC) approach to further reduce the influence of clouds, atmosphere, and solar zenith angle. The MVC method selects the largest NDVI per pixel [41-42]. The compound algorithm reduces the effect of angular and sun-target-sensor variations and provides robust spectral measures of the amount of ground vegetation, allowing precise comparison of spatiotemporal variations in terrestrial photosynthetic activity [43]. We produced monthly composites from the AVH13C1 NDVI products, using the MVC method for confirming the consistency of temporal resolution between the two NDVI

datasets. Therefore, we obtained long-term monthly NDVI data from AVH13C1 NDVI and MOD13C2 NDVI with spatial resolution 0.05°.

For land-climate studies, continuity and consistency of the two NDVI datasets are indispensable [44-45]. To evaluate their consistency in the permafrost region, we analyzed the monthly NDVI for the 1995-99 LTDR and 2000-05 MODIS datasets with corresponding parts of the 1995-2005 Global Inventory Modeling and Mapping Studies (GIMMS) dataset for the entire permafrost zone (Figs 3a and b). We also compared the annual average NDVI between LTDR and MODIS over 1982-2014, in correspondence with the GIMMS NDVI from 1982 to 2006 (Fig. 3c). The results suggest that the GIMMS NDVI was systematically underestimated (as much as 0.06) in the permafrost zone (Fig. 3a). Regression slopes between LTDR and GIMMS NDVI for 1995-99 and between MODIS and GIMMS NDVI for 2000-05 were very similar (Fig. 3b). The annual average NDVI during 1982-2006 was also very similar to that of the 1982-99 LTDR, 2000-06 MODIS, and 1982-2006 GIMMS. This result demonstrates good systematic agreement between LTDR and MODIS (Fig. 3c). The sharp increase and decrease of NDVI from the LTDR to MODIS also occurred in the GIMMS NDVI. Therefore, the long-term monthly NDVI dataset with spatial resolution 0.05° generated from LTDR and MODIS is reliable.

We calculated the mean growing-season NDVI by averaging monthly maximum values from April through October. Pixels at which the average growing-season NDVI<0.05 were masked as non-vegetated areas [27].

Climate and Vegetation Datasets

The monthly climate data for the period 1981-2014 included temperature and precipitation, and were provided by the National Meteorological Information Center of China. The data during the growing season each year were from 35 meteorological stations across the permafrost region. These data were interpolated by ArcGIS 9 software using co-Kriging based on a digital elevation model with spatial resolution 0.05°. This matched both temporally and spatially the time sequences of mean growing-season NDVI.

Vegetation data with scale 1:1,000,000 were obtained from a digitized actual vegetation map of China derived from ground-based observations [46].

Permafrost Zone in Northeastern China

The permafrost region covers 4.2×10^5 km^2. Digital data for permafrost boundaries were obtained from the U.S. National Snow and Ice Data Center (nsidc.org/data/docs/fgdc/ggd603_pf_maps_china).

Mehods

To detect vegetation and climatic variations over the 34 years, mean growing-season NDVI (MGS-NDVI), growing-season average temperature (GS-AT), and growing-season total precipitation (GS-TP) were calculated and then used as a proxy for the annual state of vegetation growth. We treated linear time trends using the ordinary least-squares regression method for NDVI and climatic factors to quantify the magnitude of those trends (Equations (1) and (2)) [18, 28, 34, 44]:

$$y = at + b + \varepsilon \tag{1}$$

$$a = \frac{\sum_{i=1}^{34}(y_i - \bar{y})(t_i - \bar{t})}{\sum_{i=1}^{34}(y_i - \bar{y})^2} \tag{2}$$

… where y is the MGS-NDVI or climate variables, t is the year, and $\bar{y}$ and $\bar{t}$ are corresponding mean values of y and t. Slope a represents the magnitude of the trend, b is the intercept, and ε is residual error. To further investigate the trends of growing-season NDVI, linear trends from 1981-2014 on a per-pixel basis were examined. The expression is [27, 44, 47-48]:
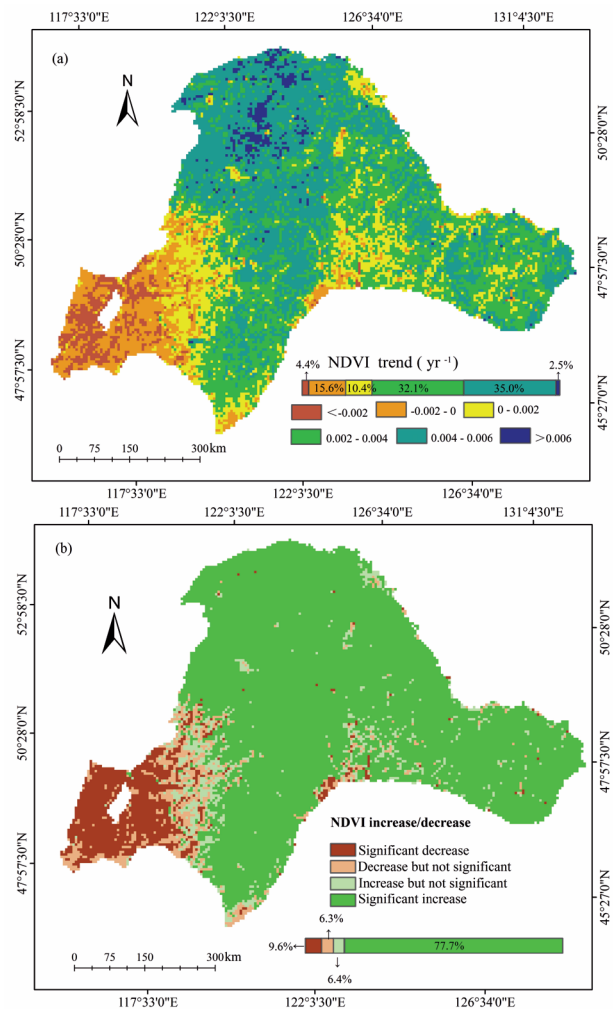

Fig. 4. Spatial distribution of mean growing-season NDVI for the permafrost zone during 1981-2014.

$$Slope = \frac{n \times \sum_{i=1}^{n} i \times \overline{NDVI}_i - \sum_{i=1}^{n} i \sum_{1}^{n} \overline{NDVI}_i}{n \times \sum_{i=1}^{n} i^2 - (\sum_{i=1}^{n} i)^2} \qquad (3)$$

...where *Slope* is the trend of vegetation dynamics or climate variables, $n = 34$, i is the number of the year (1-34) in the study period, and $NDVI_i$ is the MGS-NDVI in i the th year. The MGS-NDVI during 1981-2014 has an increasing trend when $Slope > 0$ and a decreasing trend when $Slope < 0$.

To understand the climate drivers of vegetation variables in the permafrost zone, Pearson's correlation coefficient between NDVI and climate variables was computed. Correlations range from +1 to -1. Zero correlation indicates no relationship between the variables. A negative correlation indicates that as one variable increased, the other declined. A positive correlation indicates that both variables changed in the same direction. Correlation was analyzed at both the spatial-average value scale and pixel scale (Equation (4)) [49-50]:

$$r_{xy} = \frac{\sum_{i=1}^{n}(x_i - \bar{x})(y_i - \bar{y})}{\sqrt{\sum_{i=1}^{n}(x_i - \bar{x})^2}\sqrt{\sum_{i=1}^{n}(y_i - \bar{y})^2}} \qquad (4)$$

...where r_{xy} represents the correlation coefficient for x and y, whose value is from -1 to 1, x_i and y_i are values of the two variables in the ith year, and $\bar{x}$ and $\bar{y}$ are average values of x and y during the study period, respectively.

Results

Trends of NDVI

Spatial Distribution of Vegetation Cover

The spatial pattern of MGS-NDVI is shown in Fig. 4. Overall, the MGS-NDVI was large and had obvious heterogeneity, and there was an increasing trend from west to east. Pixels with NDVI>0.6 mainly covered the Great Khingan Mountains and the southeastern area embraced the Small Khingan Mountains, which accounted for 40.5% of the permafrost area and was dominated by needleleaf, broadleaf, and mixed broadleaf and conifer forests. Moderately large values between 0.4 and 0.6 were observed in scattered areas of the central permafrost zone, which accounted for about half the study area (49.2%). There, the land was largely composed of cultivation, meadow, and swamp. Sparse vegetation cover with NDVI<0.4 was found in the temperate steppe of western areas, making up 10.3% of the study area.

Dynamics of Vegetation Cover

Fig. 5 illustrates the interannual variation of spatial average MGS-NDVI for the entire study region. This index significantly increased at a rate of 0.0028 year⁻¹ ($P < 0.001$). Spatial dynamics of the vegetation cover are
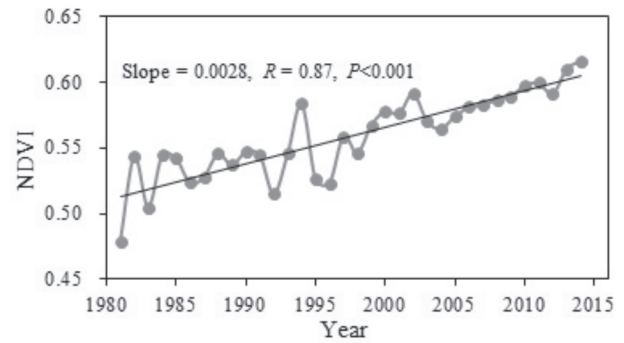

Fig. 5. Trend in spatial average growing-season mean NDVI over the entire permafrost zone of northeastern China, 1981-2014.

depicted in Fig. 6a. There was strong spatial heterogeneity from the per-pixel analysis. Pixels with increasing trends (NDVI trend>0) accounted for 80% of the permafrost area, which were mostly found across the permafrost zone, with the exception of the western steppe. Pixels with decreasing trends (NDVI trend <0) (~20% of the total area)
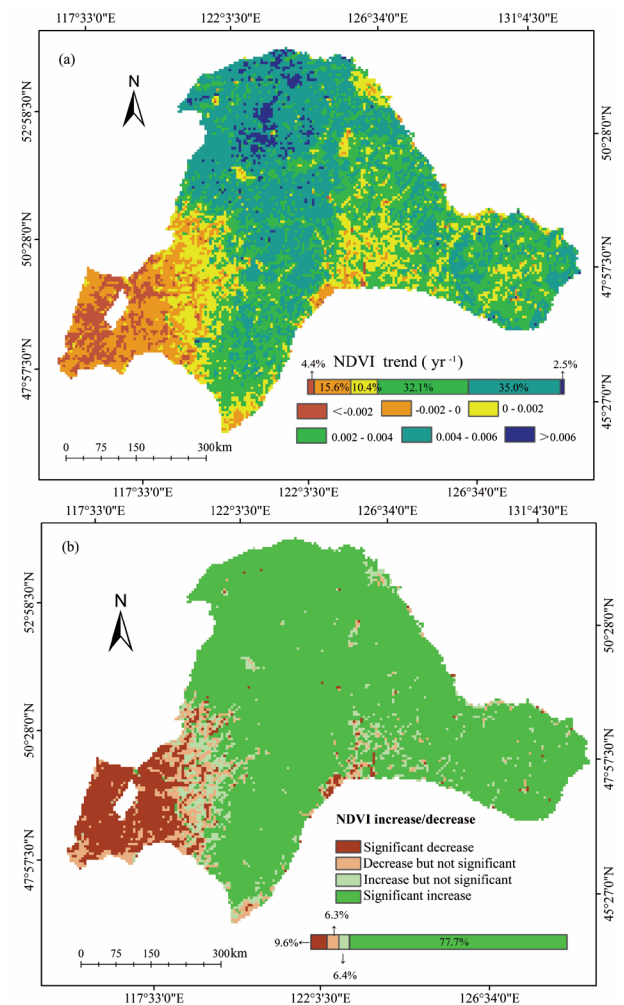

Fig. 6. Variation in mean growing-season NDVI for the permafrost zone of northeastern China, 1981-2014: a) magnitude and b) statistical test result at 5% significance level.
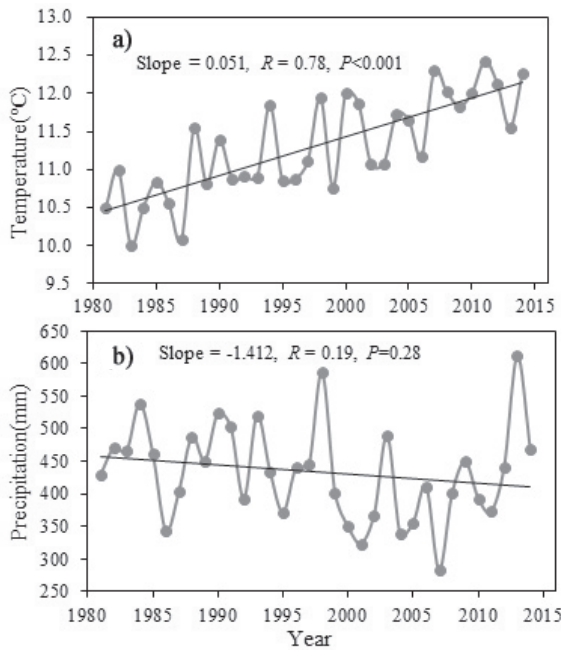
Fig. 7. Trend in spatial average growing-season a) mean temperature (ºC) and b) total precipitation (mm) in permafrost zone, 1981-2014.

Fig. 8. Variation in a) growing-season mean temperature (ºC) and b) growing-season total precipitation (mm) for permafrost zone of northeastern China, 1981-2014.

were mainly in the cultivated lands and steppe of the study area. Results of a statistical test at 5% significance level of MGS-NDVI trends are shown in Fig. 6b. The MGS-NDVI in 77.7% of the study area showed a significant increase, and only 9.6% of that area showed a significant decrease.

Trends of Climate Variables

GS-MT significantly increased at a rate of 0.051ºC/yr (Fig. 7a), consistent with the dynamic characteristics of MGS-NDVI. Fig. 7b shows the variations in GS-TP, which decreased at a rate of -1.412 mm/yr (non-significant). Spatial variations of temperature (Fig. 8a) and precipitation (Fig. 8b) at pixel scale showed great spatial heterogeneity across the permafrost zone. In the Great Khingan Mountains and central parts of the Small Khingan Mountains, which are mainly covered by forest, temperature increased at the highest average rates. However, the greatest precipitation decreases in the study area were found in the southeastern Small Khingan Mountains.

Correlation between Vegetation Dynamics and Climate Factors

Correlation between Growing-Season Mean NDVI and Climate Variables at the Scale of the Entire Permafrost Zone

At the entire permafrost zone scale we analyzed the correlation between the MGS-NDVI and climate variables. The MGS-NDVI was positively and significantly correlated with GS-MT *(R = 0.779; P<0.01)*, but
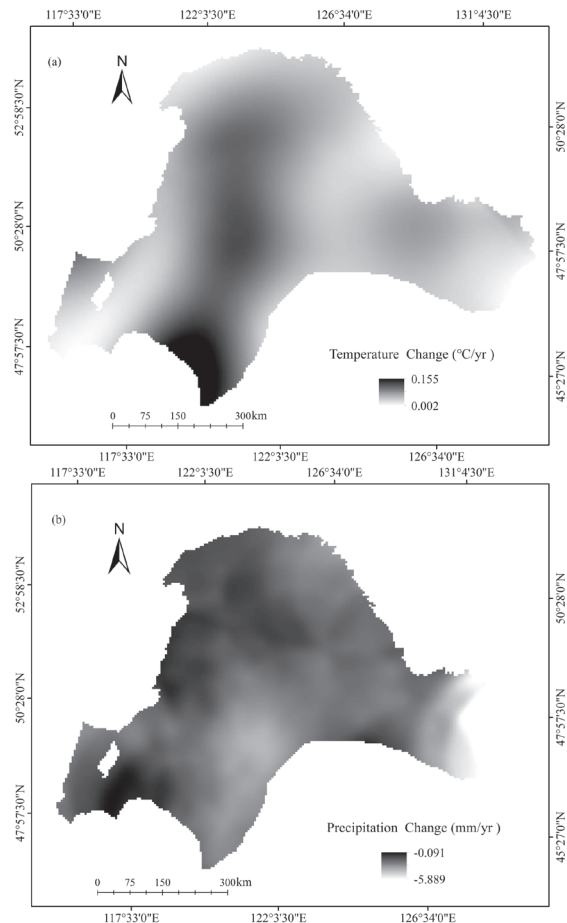
weakly and negatively related with GS-TP (*R* = -0.086; *P* = 0.103). We compared correlation coefficients between MGS-NDVI and climate variables, finding that correlation between MGS-NDVI and GS-MT was much stronger than between MGS-NDVI and GS-TP. Thus, we conclude that GS-MT was the primary determinant of vegetation dynamics in the permafrost zone of northeastern China.

Correlation between Growing-Season Mean NDVI and Climate Factors at Pixel Scale

To further assess correlations between MGS-NDVI and climate variables, we calculated correlation coefficients between MGS-NDVI and the two climate factors at all pixels (Fig. 9). There was strong and positive correlation between MGS-NDVI and GS-MT in most permafrost areas, which constituted ~68.2% of the total permafrost area (1% and 5% significance levels). Especially in the central and eastern permafrost zone where there were large NDVI values and extensive forest cover, correlation was significant even at the 0.01 level (~59.4%) (Fig. 9a). However, in the steppe-dominated areas of the western study area, GS-MT had significant and negative correlation with MGS-NDVI, at ~8.5% of all pixels.

Compared with the correlation between MGS-NDVI and GS-MT, there was an opposite spatial pattern of correlation between MGS-NDVI and GS-TP (Fig. 9b), i.e., strong and positive correlation was mainly in the western study area that was covered by steppe, accounting for 17.8% of all pixels. Correlation between MGS-NDVI and GS-TP was weakly negative in most parts of permafrost zone (~77.9%). Significant negative correlation was found in some scattered parts of the permafrost zone (~4.3%).

Discussion

Trends of Growing-Season Mean NDVI (MGS-NDVI)

As the most active stage in the entire phenology cycle of non-evergreen vegetation [51], the growing season is often used to detect vegetation dynamics. Therefore, MGS-NDVI was an effective indicator of vegetation variation conditions [18]. The combination of climate and vegetation during the growing season suggests
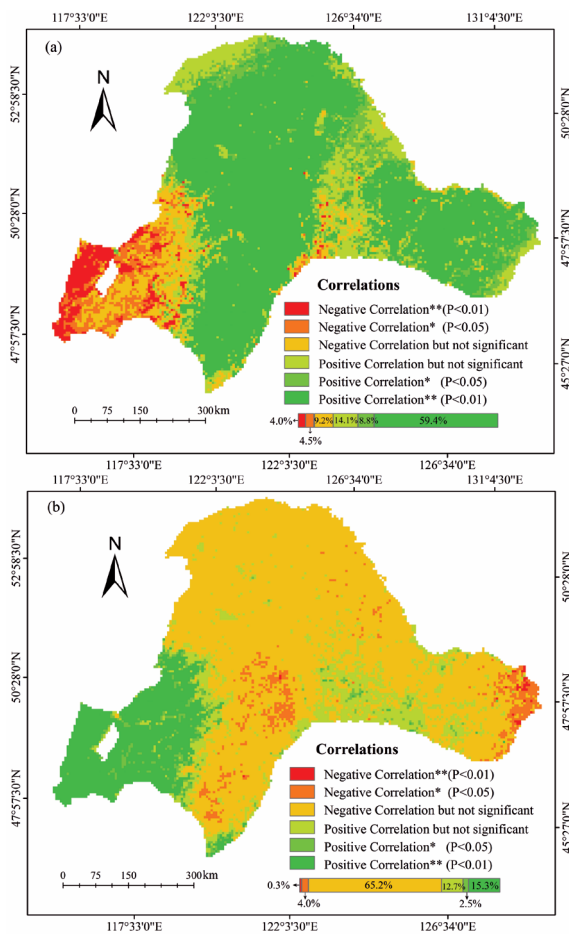

Fig. 9. Correlations between mean NDVI and climate variables of growing season: a) correlations between NDVI and mean temperature and b) correlations between NDVI and total precipitation in permafrost zone of northeastern China, 1981-2014.
* and ** denote 5% and 1% significance levels, respectively.

that vegetation dynamics have significantly increased on global and regional scales [16, 32, 35, 52-58]. For example, Piao et al. indicated a significant ($R = 0.768$; $P<0.001$) increasing trend of growing-season NDVI on the national scale, with an annual increase rate of 0.0015 year^{-1} over 1982-99 [33]. In the permafrost areas, vegetation variations of net primary productivity and vegetation cover increased significantly [26, 50, 59] and are consistent with our results, which show that MGS-NDVI had a significant increasing trend with a rate of 0.0028 year^{-1} in the permafrost zone of northeastern China during 1981-2014.

Correlations of Growing-Season mean NDVI and Climate Variables

Vegetation changes were strongly correlated with climate variables [60-62]. At the scale of the entire permafrost zone, the MGS-NDVI was positively and significantly correlated with GS-MT ($R = 0.779$; $P<0.01$), but weakly and negatively related to GS-TP ($R = -0.086$; $P = 0.103$). The correlation between MGS-NDVI and climate factors (temperature and precipitation) on the scale of the entire permafrost zone suggests that vegetation growth was greatly influenced by GS-MT, consistent with the results of previous studies [27, 63-66]. The permafrost zone of northeastern China is in a cold region, where the positive and significant correlation can be physiologically explained by an increase of temperature accelerating plant photosynthesis [33].

The spatial pattern of per-pixel correlation between MGS-NDVI and climate variables showed strong heterogeneity. The positive correlation between MGS-NDVI and GS-MT in most parts of the permafrost zone (except for the west) is attributed to an increased growing-season temperature. This enhanced vegetation photosynthesis comes with an extended growing season and increased plant activity (amplitude of the growth cycle) [67-69]. This can be interpreted as an increase in photosynthesis and respiration for vegetation growth in response to a warmer climate [66]. Negative correlation between MGS-NDVI and GS-MT was observed in the western study area (Hulun Buir grassland), because increased temperature limited plant growth in these semiarid regions. In such a region, increased temperature may reduce moisture availability for vegetation growth [33, 44]. Increasing GS-MT invigorated transpiration and indicates that vegetation cover decreases with increasing temperature during the growing season. However, the correlation between MGS-NDVI and GS-TP showed a spatial pattern opposite that of the correlation between MGS-NDVI and GS-MT. Significant positive correlation between MGS-NDVI and GS-TP in the western permafrost zone is attributed to water availability in this semiarid region, which is the primary limiting factor for plant growth [20]. The decreasing vegetation cover in the Hulun Buir grassland was caused by declining GS-TP, which reduced effective moisture for vegetation

growth [44]. Additionally, there was non-significant negative correlation between MGS-NDVI and GS-TP in most permafrost areas, where the climate in the growing season is cold and humid [70]. Apparently in these areas, increased precipitation is associated with greater cloud cover that reduces incident radiation and which is essential for plant growth [33, 44, 62]. However, seasonal freezing and thawing of the permafrost provided sufficient moisture for vegetation growth in areas insensitive to variations of precipitation.

Conclusions

In this paper, we reveal spatiotemporal variations in vegetation cover and the correlation between vegetation and climate variables. The main conclusions are:

1. The MGS-NDVI significantly increased at a rate of 0.0028 year^{-1} at the scale of the entire permafrost zone. Spatial dynamics of the vegetation cover in the permafrost zone had strong heterogeneity at pixel scale.

2. At the scale of the entire permafrost zone, the NDVI is positively and significantly correlated with temperature, but weakly and negatively related to precipitation. This indicates that temperature was the dominant influence on vegetation growth during the growing season.

Although the results of the present study are valuable, there are several aspects that remain unclear and must be addressed in the future. For example, despite a strong NDVI increase in the permafrost zone of northeastern China over the last three decades, we still do not understand carbon exchange in the zone under the background of climate change. More studies are needed to assess the role of this zone in regional carbon balance. In addition to climate variables, CO_2 and human activities may also influence NDVI change. We should consider other available data of variables affecting vegetation growth. Finally, we will examine the effect of permafrost degradation on vegetation growth.

Acknowledgments

Author Contributions

Jinting Guo: substantial contributions toward the collection, processing, analysis, and interpretation of data, plus manuscript preparation; Yuanman Hu: ensured integrity of the entire study; Zaiping Xiong: guidance for the ArcGIS software; Xiaolu Yan: data analysis; Baihui Ren: data collection; Rencang Bu: manuscript review and final approval of the version for publication.

References

1. ANDERSON R.G., CANADELL J.G., RANDERSON J.T., JACKSON R.B., HUNGATE B.A., BALDOCCHI D.D., BAN-WEISS G.A., BONAN G.B., CALDEIRA K., CAO L., DIFFENBAUGH N.S., GURNEY K.R., KUEPPERS L.M., LAW B.E., LUYSSAERT S., O'HALLORAN T.L. Biophysical considerations in forestry for climate protection. Front. in Ecol. Environ. **9**, 174, **2011**.

2. BALLING R.C., KLOPATEK J.M., HILDEBRANDT M.L., MORITZ C.K., WATTS C.J. Impacts of land degradation on historical temperature records from the sonoran desert. Climatic Change **40**, 669, **1998**.

3. JACKSON R.B., RANDERSON J.T., CANADELL J.G., ANDERSON R.G., AVISSAR R., BALDOCCHI D.D., BONAN G.B., CALDEIRA K., DIFFENBAUGH N.S., FIELD C.B., HUNGATE B.A., JOBBAGY E.G., KUEPPERS L.M., NOSETTO M.D., PATAKI D.E. Protecting climate with forests. Environ. Res. Lett. **3**, 044006, **2008**.

4. SCHWALM C.R., WILLIAMS C.A., SCHAEFER K., ARNETH A., BONAL D., BUCHMANN N., CHEN J., LAW B.E., LINDROTH A., LUYSSAERT S., REICHSTEIN M., RICHARDSON A.D. Assimilation exceeds respiration sensitivity to drought: A fluxnet synthesis. Global Change Biol. **16**, 657, **2010**.

5. ICHII K., KAWABATA A., YAMAGUCHI Y. Global correlation analysis for NDVI and climatic variables and NDVI trends: 1982-1990. Int. J. Remote Sens. **23**, 3873, **2002**.

6. JIANG D.J., FU X.F., WANG K. Vegetation dynamics and their response to freshwater inflow and climate variables in the yellow river delta, china. Quatern. Int. **304**, 75, **2013**.

7. SARKAR S., KAFATOS M. Interannual variability of vegetation over the Indian sub-continent and its relation to the different meteorological parameters. Remote Sens. Environ. **90**, 268, **2004**.

8. ZHONG L., MA Y.M., SALAMA M.S., SU Z.B. Assessment of vegetation dynamics and their response to variations in precipitation and temperature in the tibetan plateau. Climatic Change **103**, 519, **2010**.

9. BROWN M.E., DE BEURS K., VRIELING A. The response of african land surface phenology to large scale climate oscillations. Remote Sens. Environ. **114**, 2286, **2010**.

10. CHEN X.Q., HU B., YU R. Spatial and temporal variation of phenological growing season and climate change impacts in temperate eastern china. Global Change Biol. **11**, 1118, **2005**.

11. CONG N., WANG T., NAN H.J., MA Y.C., WANG X.H., MYNENI R.B., PIAO S.L. Changes in satellite-derived spring vegetation green-up date and its linkage to climate in china from 1982 to 2010: A multimethod analysis. Global Change Biol. **19**, 881, **2013**.

12. LIU Q., FU Y.S.H., ZENG Z.Z., HUANG M.T., LI X.R., PIAO S.L. Temperature, precipitation, and insolation effects on autumn vegetation phenology in temperate china. Global Change Biol. **22**, 644, **2016**.

13. MOULIN S., KERGOAT L., VIOVY N., DEDIEU G. Global-scale assessment of vegetation phenology using

noaa/avhrr satellite measurements. J. Climate **10**, 1154, **1997**.

14. ANAV A., FRIEDLINGSTEIN P., BEER C., CIAIS P., HARPER A., JONES C., MURRAY-TORTAROLO G., PAPALE D., PARAZOO N.C., PEYLIN P., PIAO S.L., SITCH S., VIOVY N., WILTSHIRE A., ZHAO M.S. Spatiotemporal patterns of terrestrial gross primary production: A review. Rev. Geophys. **53**, 785, **2015**.

15. MELILLO J.M., MCGUIRE A.D., KICKLIGHTER D.W., MOORE B., VOROSMARTY C.J., SCHLOSS A.L. Global climate change and terrestrial net primary production. Nature **363**, 234, **1993**.

16. NEMANI R.R., KEELING C.D., HASHIMOTO H., JOLLY W.M., PIPER S.C., TUCKER C.J., MYNENI R.B., RUNNING S.W. Climate-driven increases in global terrestrial net primary production from 1982 to 1999. Science **300**, 1560, **2003**.

17. PIAO S.L., FANG J.Y., ZHOU L.M., ZHU B., TAN K., TAO S. Changes in vegetation net primary productivity from 1982 to 1999 in china. Global Biogeochem. Cy. **19**, 19, **2005**.

18. PIAO S.L., FANG J.Y., ZHOU L.M., GUO Q.H., HENDERSON M., JI W., LI Y., TAO S. Interannual variations of monthly and seasonal normalized difference vegetation index (NDVI) in china from 1982 to 1999. J. Geophys. Res. **108**, 13, **2003**.

19. STOW D.A., HOPE A., MCGUIRE D., VERBYLA D., GAMON J., HUEMMRICH F., HOUSTON S., RACINE C., STURM M., TAPE K., HINZMAN L., YOSHIKAWA K., TWEEDIE C., NOYLE B., SILAPASWAN C., DOUGLAS D., GRIFFITH B., JIA G., EPSTEIN H., WALKER D., DAESCHNER S., PETERSEN A., ZHOU L., MYNENI R. Remote sensing of vegetation and land-cover change in arctic tundra ecosystems. Remote Sens. Environ. **89**, 281, **2004**.

20. SUN W.Y., SONG X.Y., MU X.M., GAO P., WANG F., ZHAO G.G. Spatiotemporal vegetation cover variations associated with climate change and ecological restoration in the loess plateau. Agr. Forest Meteorol. **209**, 87, **2015**.

21. XIN Z.B., XU J.X., ZHENG W. Spatiotemporal variations of vegetation cover on the chinese loess plateau (1981-2006): Impacts of climate changes and human activities. Sci. China Ser. D **51**, 67, **2008**.

22. YANG Y., XU J.H., HONG Y.L., LV G.G. The dynamic of vegetation coverage and its response to climate factors in inner mongolia, china. Stoch. Environ. Res. Risk Assess. **26**, 357, **2012**.

23. DONG J.R., KAUFMANN R.K., MYNENI R.B., TUCKER C.J., KAUPPI P.E., LISKI J., BUERMANN W., ALEXEYEV V., HUGHES M.K. Remote sensing estimates of boreal and temperate forest woody biomass: Carbon pools, sources, and sinks. Remote Sens. Environ. **84**, 393, **2003**.

24. PARTON W.J., SCURLOCK J.M.O., OJIMA D.S., GILMANOV T.G., SCHOLES R.J., SCHIMEL D.S., KIRCHNER T., MENAUT J.C., SEASTEDT T., MOYA E.G., KAMNALRUT A., KINYAMARIO J.I. Observations and modeling of biomass and soil organic-matter dynamics for the grassland biome worldwide. Global Biogeochem. Cy. **7**, 785, **1993**.

25. SCHIMEL D.S., HOUSE J.I., HIBBARD K.A., BOUSQUET P., CIAIS P., PEYLIN P., BRASWELL B.H., APPS M.J., BAKER D., BONDEAU A., CANADELL J., CHURKINA G., CRAMER W., DENNING A.S., FIELD C.B., FRIEDLINGSTEIN P., GOODALE C., HEIMANN M., HOUGHTON R.A., MELILLO J.M., MOORE B., MURDIYARSO D., NOBLE I., PACALA S.W., PRENTICE I.C., RAUPACH M.R., RAYNER P.J., SCHOLES R.J., STEFFEN W.L., WIRTH C. Recent patterns and mechanisms of carbon exchange by terrestrial ecosystems. Nature **414**, 169, **2001**.

26. YANG Z.P., GAO J.X., ZHOU C.P., SHI P.L., ZHAO L., SHEN W.S., OUYANG H. Spatio-temporal changes of NDVI and its relation with climatic variables in the source regions of the yangtze and yellow rivers. J. Geogr. Sci. **21**, 979, **2011**.

27. LIU X.F., ZHU X.F., LI S.S., LIU Y.X., PAN Y.Z. Changes in growing season vegetation and their associated driving forces in china during 2001-2012. Remote Sens. **7**, 15517, **2015**.

28. PIAO S.L, WANG X.H., CIAIS P., ZHU B., WANG T., LIU J. Changes in satellite-derived vegetation growth trend in temperate and boreal eurasia from 1982 to 2006. Global Change Biol. **17**, 3228, **2011**.

29. ZHOU L., TUCKER C.J., KAUFMANN R.K., SLAYBACK D., SHABANOV N.V., MYNENI R.B. Variations in northern vegetation activity inferred from satellite data of vegetation index during 1981 to 1999. J. Geophys. Res. **106**, 20069, **2001**.

30. WEI Z., JIN H.J., ZHANG J.M., YU S.P., HAN X.J., JI Y.J., HE R.X., CHANG X.L. Prediction of permafrost changes in northeastern china under a changing climate. Sci. China-Earth Sci. **54**, 924, **2011**.

31. JIN H.J., YU Q.H., LII L.Z., GUO D.X., HE R.X., YU S.P., SUN G.Y., LI Y.W. Degradation of permafrost in the xing'anling mountains, northeastern china. Permafrost Periglacial **18**, 245, **2007**.

32. FANG J.Y., PIAO S.L., HE J.S., MA W.H. Increasing terrestrial vegetation activity in china, 1982-1999. Sci. China Ser. C-Life Sci. **47**, 229, **2004**.

33. PIAO S.L., FANG J.Y., JI W., GUO Q.H., KE J.H., TAO S. Variation in a satellite-based vegetation index in relation to climate in china. J. Veg. Sci. **15**, 219, **2004**.

34. BAO G., QIN Z.H., BAO Y.H., ZHOU Y., LI W.J., SANJJAV A. NDVI-based long-term vegetation dynamics and its response to climatic change in the mongolian plateau. Remote Sens. **6**, 8337, **2014**.

35. PIAO S.L., FRIEDLINGSTEIN P., CIAIS P., ZHOU L.M., CHEN A.P. Effect of climate and CO2 changes on the greening of the northern hemisphere over the past two decades. Geophys. Res. Lett. **33**, L23402, **2006**.

36. KIDWELL K.B. Noaa polar orbiter data user's guide (tiros-n, noaa-6, noaa-7, noaa-8, noaa-9, noaa-10, noaa-11, noaa-12, noaa-13 and noaa-14). National Oceanic and Atmospheric Administration, Washington D.C. 1998. http://www.ncdc.noaa.gov/oa/pod-guide/ncdc/docs/podug/index.htm.

37. PEDELTY J., DEVADIGA S., MASUOKA E., BROWN M., PINZON J., TUCKER C., VERMOTE E., PRINCE S., NAGOL J., JUSTICE C., ROY D., JUNCHANG J., SCHAAF C., JICHENG L., PRIVETTE J., PINHEIRO A. Generating a long-term land data record from the AVHRR and MODIS instruments. IEEE International Geoscience and Remote Sensing Symposium, **2007**.

38. FENSHOLT R., PROUD S.R. Evaluation of earth observation based global long term vegetation trends-comparing GIMMS and MODIS global NDVI time series. Remote Sens. Environ. **119**, 131, **2012**.

39. GUO M., WANG X.F., LI J., YI K.P., ZHONG G.S., TANI H. Assessment of global carbon dioxide concentration using modis and gosat data. Sensors **12**, 16368, **2012**.

40. SOLANO R., DIDAN, K., JACOBSON, A., & HUETE A. Modis vegetation indices (MOD13) c5 user's guide. 2010. Available at: http://tbrs.arizona.edu/project/MODIS/UsersGuide.pdf.

41. HOLBEN B.N. Characteristics of maximum-value composite images from temporal AVHRR data. Int. J. Remote Sens. **7**, 1417, **1986**.

42. HUETE A., JUSTICE C., VAN LEEUWEN W. Modis vegetation index (mod13). Algorithm theoretical basis document. 1999.

43. HUETE A., DIDAN K., MIURA T., RODRIGUEZ E.P., GAO X., FERREIRA L.G. Overview of the radiometric and biophysical performance of the MODIS vegetation indices. Remote Sens. Environ. **83**, 195, **2002**.

44. MAO D.H., WANG Z.M., LUO L., REN C.Y. Integrating AVHRR and MODIS data to monitor NDVI changes and their relationships with climatic parameters in northeast china. Int. J. Appl. Earth Obs. **18**, 528, **2012**.

45. STEVEN M.D., MALTHUS T.J., BARET F., XU H., CHOPPING M.J. Intercalibration of vegetation indices from different sensor systems. Remote Sens. Environ. **88**, 412, **2003**.

46. Editorial board of vegetation map of china, Chinese Academy of Sciences (EBVMC). Vegetation atlas of china, Science Press, beijing, **2001** [In Chinese].

47. LIU X.F., ZHANG J.S., ZHU X.F., PAN Y.Z., LIU Y.X., ZHANG D.H., LIN Z.H. Spatiotemporal changes in vegetation coverage and its driving factors in the three-river headwaters region during 2000-2011. J. Geogr. Sci. **24**, 288, **2014**.

48. STOW D., DAESCHNER S., HOPE A., DOUGLAS D., PETERSEN A., MYNENI R., ZHOU L., OECHEL W. Variability of the seasonally integrated normalized difference vegetation index across the north slope of alaska in the 1990s. Int. J. Remote Sens. **24**, 1111, **2003**.

49. HERRMANN S.M., ANYAMBA A., TUCKER C.J. Recent trends in vegetation dynamics in the african sahel and their relationship to climate. Global Environ. Change **15**, 394, **2005**.

50. MAO D.H., LUO L.L., WANG Z.M., ZHANG C.H., REN C.Y. Variations in net primary productivity and its relationships with warming climate in the permafrost zone of the tibetan plateau. J. Geogr. Sci. **25**, 967, **2015**.

51. JONG R.D., BRUIN S.D., WIT A.D., SCHAEPMAN M.E., DENT D.L. Analysis of monotonic greening and browning trends from global ndvi time-series. Remote Sens. Environ. **115**, 692, **2011**.

52. DENG S.F., YANG T.B., ZENG B., ZHU X.F., XU H.J. Vegetation cover variation in the qilian mountains and its response to climate change in 2000-2011. J. Mt. Sci-Engl. **10**, 1050, **2013**.

53. MYNENI R.B., KEELING C.D., TUCKER C.J., ASRAR G., NEMANI R.R. Increased plant growth in the northern high latitudes from 1981 to 1991. Nature **386**, 698, **1997**.

54. PENG S.S., CHEN A.P., XU L., CAO C.X., FANG J.Y., MYNENI R.B., PINZON J.E., TUCKER C.J., PIAO S.L. Recent change of vegetation growth trend in china. Environ. Res. Lett. **6**, 044027, **2011**.

55. TUCKER C.J., SLAYBACK D.A., PINZON J.E., LOS S.O., MYNENI R.B., TAYLOR M.G. Higher northern latitude normalized difference vegetation index and growing season trends from 1982 to 1999. Int. J. Biometeorol. **45**, 184, **2001**.

56. XU X., CHEN H., LEVY J.K. Spatiotemporal vegetation cover variations in the qinghai-tibet plateau under global climate change. Chinese Sci. Bull. **53**, 915, **2008**.

57. ZHAO M.S., RUNNING S.W. Drought-induced reduction in global terrestrial net primary production from 2000 through 2009. Science **329**, 940, **2010**.

58. ZHOU D.W., FAN G.Z., HUANG R.H., FANG Z.F., LIU Y.Q., LI H.Q. Interannual variability of the normalized difference vegetation index on the tibetan plateau and its relationship with climate change. Adv. Atmos. Sci. **24**, 474, **2007**.

59. RAYNOLDS M.K., WALKER D.A., VERBYLA D., MUNGER C.A. Patterns of change within a tundra landscape: 22-year landsat ndvi trends in an area of the northern foothills of the brooks range, alaska. Arct. Antarct. Alp. Res. **45**, 249, **2013**.

60. GOETZ S.J., BUNN A.G., FISKE G.J., HOUGHTON R.A. Satellite-observed photosynthetic trends across boreal north america associated with climate and fire disturbance. P. Natl. Acad. Sci. USA. **102**, 13521, **2005**.

61. PIAO S.L., CIAIS P., HUANG Y., SHEN Z.H., PENG S.S., LI J.S., ZHOU L.P., LIU H.Y., MA Y.C., DING Y.H., FRIEDLINGSTEIN P., LIU C.Z., TAN K., YU Y.Q., ZHANG T.Y., FANG J.Y. The impacts of climate change on water resources and agriculture in china. Nature. **46**, 743, **2010**.

62. SONG Y., MA M.G. A statistical analysis of the relationship between climatic factors and the normalized difference vegetation index in china. Int. J. Remote Sens. **32**, 3947, **2011**.

63. FANG J.Y., PIAO S.L., FIELD C.B., PAN Y.D., GUO Q.H., ZHOU L.M., PENG C.H., TAO S. Increasing net primary production in china from 1982 to 1999. Front. Ecol. Environ. **12**, 93, **2003**.

64. LOTSCH A., FRIEDL M.A., ANDERSON B.T., TUCKER C.J. Response of terrestrial ecosystems to recent northern hemispheric drought. Geophys. Res. Lett. **32**, L06705, **2005**.

65. MYNENI R.B., DONG J., TUCKER C.J., KAUFMANN R.K., KAUPPI P.E., LISKI J., ZHOU L., ALEXEYEV V., HUGHES M.K. A large carbon sink in the woody biomass of northern forests. P. Natl. Acad. Sci. USA. **98**, 14784, **2001**.

66. PIAO S.L., NAN H.J., HUNTINGFORD C., CIAIS P., FRIEDLINGSTEIN P., SITCH S., PENG S., AHLSTROM A., CANADELL J.G., CONG N., LEVIS S., LEVY P.E., LIU L.L., LOMAS M.R., MAO J.F., MYNENI R.B., PEYLIN P., POULTER B., SHI X.Y., YIN G.D., VIOVY N., WANG T., WANG X.H., ZAEHLE S., ZENG N., ZENG Z.Z., CHEN A.P. Evidence for a weakening relationship between interannual temperature variability and northern vegetation activity. Nat. Commun. **5**, 5018, **2014**.

67. JEONG S.J., HO C.H., GIM H.J., BROWN M.E. Phenology shifts at start vs. End of growing season in temperate vegetation over the northern hemisphere for the period 1982-2008. Global Change Biol. **17**, 2385, **2011**.

68. LOS S.O., COLLATZ G.J., BOUNOUA L., SELLERS P.J., TUCKER C.J. Global interannual variations in sea surface temperature and land surface vegetation, air temperature, and precipitation. J. Climate **14**, 1535, **2001**.

69. XU L., MYNENI R.B., CHAPIN F.S., III, CALLAGHAN T.V., PINZON J.E., TUCKER C.J., ZHU Z., BI J., CIAIS P., TOMMERVIK H., EUSKIRCHEN E.S., FORBES B.C., PIAO S.L., ANDERSON B.T., GANGULY S., NEMANI R.R., GOETZ S.J., BECK P.S.A., BUNN A.G., CAO C., STROEVE J.C. Temperature and vegetation seasonality diminishment over northern lands. Nat. Clim. Change **3**, 581, **2013**.

70. FANG J.Y., YODA K. Climate and vegetation in china iii water balance and distribution of vegetation. Ecol. Re. **5**, 9, **1990**.